Materials Today Physics 13 (2020) 100194

Contents lists available at ScienceDirect

Materials Today Physics

journal homepage: https://www.journals.elsevier.com/materials-today-physics

Photoluminescence mapping and time-domain thermo-photoluminescence for rapid imaging and measurement of thermal conductivity of boron arsenide

S. Yue [a, b, 1], G.A. Gamage [c, 1], M. Mohebinia [d], D. Mayerich [b], V. Talari [e], Y. Deng [e], F. Tian [c], S.-Y. Dai [f, b], H. Sun [c], V.G. Hadjiev [g], W. Zhang [h], G. Feng [f], J. Hu [h], D. Liu [e], Z. Wang [a, **], Z. Ren [c, ***], J. Bao [b, d, *]

[a] Institute of Fundamental and Frontier Sciences, University of Electronic Science and Technology of China, Chengdu, Sichuan, 610054, China
[b] Department of Electronic and Computer Engineering, University of Houston, Houston, TX, 77204, USA
[c] Department of Physics and Texas Center for Superconductivity, University of Houston, Houston, TX, 77204, USA
[d] Materials Science & Engineering, University of Houston, Houston, TX, 77204, USA
[e] Department of Mechanical Engineering, University of Houston, Houston, TX, 77204, USA
[f] College of Electronics & Information Engineering, Sichuan University, Chengdu, Sichuan, 610064, China
[g] Texas Center for Superconductivity, University of Houston, Houston, TX, 77204, USA
[h] Department of Electrical and Computer Engineering, Baylor University, Waco, TX, 76798, USA

ARTICLE INFO

Article history:
Received 8 January 2020
Received in revised form
12 February 2020
Accepted 12 February 2020
Available online 21 February 2020

Keywords:
Boron arsenide
Band gap
Photoluminescence mapping
Time-domain thermo-photoluminescence
Thermal conductivity

ABSTRACT

Cubic boron arsenide (BAs) is attracting greater attention owing to the recent experimental demonstration of ultrahigh thermal conductivity κ higher than 1000 W/m·K. However, its bandgap has not been settled and a simple yet effective method to probe its crystal quality is missing. Furthermore, traditional κ measurement methods are destructive and time consuming, thus they cannot meet the urgent demand for fast screening of high κ materials. After we experimentally established 1.82 eV as the indirect bandgap of BAs and observed room-temperature band-edge photoluminescence, we developed two new optical techniques that can provide rapid and non-destructive characterization of κ with little sample preparation: photoluminescence mapping (PL-mapping) and time-domain thermo-photoluminescence (TDTP). PL-mapping provides nearly real-time image of crystal quality and κ over mm-sized crystal surfaces; while TDTP allows us to pick up any spot on the sample surface and measure its κ using nanosecond laser pulses. These new techniques reveal that the apparent single crystals are not only non-uniform in κ but also are made of domains of very distinct κ. Because PL-mapping and TDTP are based on the band-edge PL and its dependence on temperature, they can be applied to other semiconductors, thus paving the way for rapid identification and development of high-κ semiconducting materials.

1. Introduction

Cubic boron arsenide (BAs) is one of the most difficult crystals to synthesize owing to the inertness of boron (B), high toxicity of arsenic (As), very high melting point of B (~2076 °C), very low sublimation point of As (~615 °C), and the decomposition of BAs into $B_{12}As_2$ at about 920 °C [1–3]. The interest in BAs increased suddenly in 2013 when first-principles calculations predicted BAs as a highly thermal conductive (κ) material with a value comparable with that of diamond and much higher than the most commonly used heat-sink materials such as copper and silicon carbide [4,5]. Subsequent intense research led to successful synthesis and verification of the predicted high-κ material in 2018 by three groups, opening up new opportunities for more basic research, as well as potential applications [6–8]. Considering the current overheating trade-off caused by the increased power density of modern transistors, BAs could provide an opportunity to upgrade for the

* Corresponding author.
** Corresponding author.
*** Corresponding author.
E-mail addresses: zhmwang@uestc.edu.cn (Z. Wang), zren@uh.edu (Z. Ren), jbao@uh.edu (J. Bao).
[1] These authors contributed equally to this work.

https://doi.org/10.1016/j.mtphys.2020.100194
2542-5293/

semiconductor industry in the near future [9]. At the same time, its predicted high carrier mobility also holds promising potential for high-performance multifunctional next-generation electronic devices [10]. However, despite BAs being first studied in the late 50s of the last century [1], its actual bandgap value has not been well settled. The bandgap from the latest first-principles DFT calculations by several independent groups begins to merge but still falls in a wide range from 1.7 to 2.1 eV [11–14]. The bandgaps from earlier calculations were too low (1.0 eV–0.3 eV) [15,16]. Experimentally, earlier studies put the bandgap down to 1.4–1.5 eV [3,17,18]; latest low temperature photoluminescence (PL) combined with hybrid functional calculations brought the bandgap up to 1.78 eV [12]. More experiments are needed to confirm the bandgap, and a direct experimental measurement of BAs bandgap is still missing.

In addition to the uncertainty in its basic bandgap, current κ measurement methods are difficult to meet the demand for rapid screening of κ for development of BAs for future device applications. X-ray diffraction and transmission electron microscopy were used to prove the high crystal quality of BAs in recent demonstrations [6–8], but it is well known that these techniques are not very sensitive to impurities, point defects, and doping levels, which are important for phonon dynamics and transport [4,5]. Time-domain thermoreflectance (TDTR) was used by all three groups to determine κ of BAs [6–8], but it is a very specialized technique that requires expensive lasers, sophisticated data collection, analysis and interpretation [19–22]. TDTR also requires a complicated sample preparation step: the surface of the sample must be polished to be flat enough and is then coated with a metal film that serves as both a laser absorber and a thermal transducer [19–22]. Other methods, such as one-dimensional heat transport method coupled with Raman temperature sensing, require even more careful sample preparation, so they are not widely used [6]. It should be noted that κ is much harder and more challenging to measure than temperature, especially for high κ materials because it involves rapid local material heating and temperature sensing.

In this work, we first experimentally determine the BAs bandgap using optical absorption spectroscopy and then report the observation of room-temperature band-edge PL. Based on the relationship of PL with crystal quality and temperature, we develop and demonstrate two new optical techniques that can produce rapid non-intrusive imaging of κ over a large region with micrometer spatial resolution with little sample preparation: photoluminescence mapping (PL-mapping) and time-domain thermo-photoluminescence (TDTP). PL-mapping can generate 2D images of κ within seconds and even in real-time. TDTP uses two pump-pulse nanosecond lasers to determine κ from an arbitrary spot of a sample surface. Because PL-mapping and TDTP use simple lasers, they are accessible by many researchers, thus will greatly accelerate the pace of discovery, development, and applications of semiconductor-based high κ materials.

2. Results and discussion

Bandgap is the most important property of a semiconductor, it is also an essential parameter for theoretical calculation and forms the basis for optical, electronic, as well as thermal properties [23]. To experimentally obtain BAs bandgap, we grew thin single crystals using a recently reported method and chose optical absorption spectroscopy to directly measure its bandgap [24–26]. Fig. 1a shows UV-Visible absorption spectra of three representative samples at room temperature in Tauc plot as an indirect semiconductor. The nature of indirect bandgap semiconductor is quickly confirmed because despite their differences in absorption at lower energy tails, all of them exhibit the same and well-defined absorption

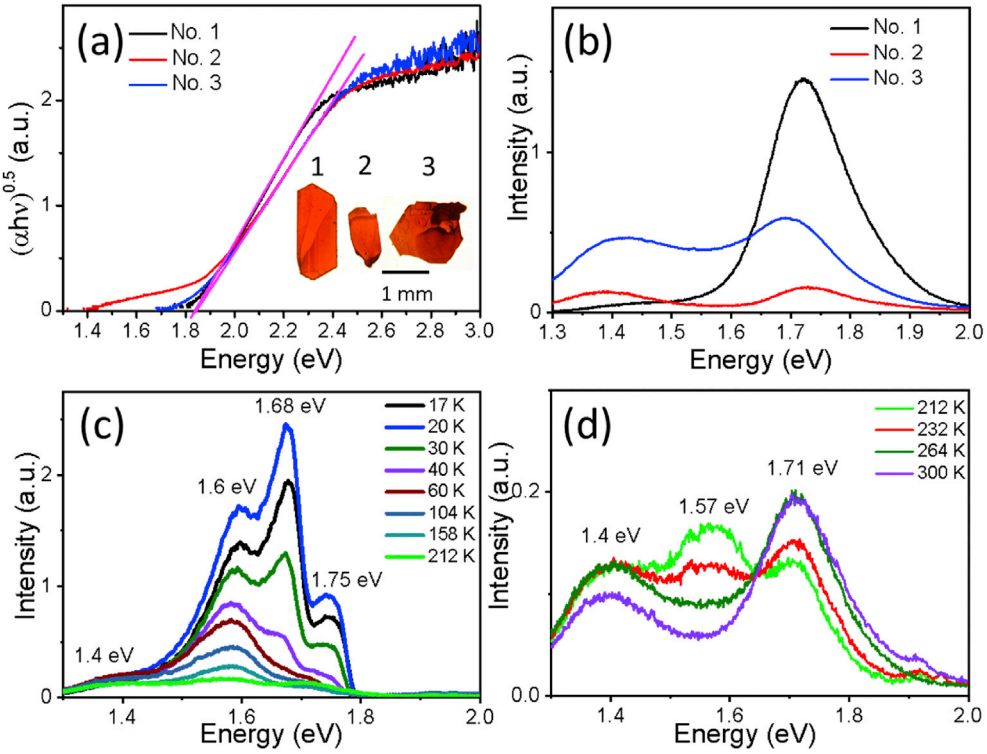

Fig. 1. Optical absorption and photoluminescence spectra of BAs crystals. (a) Indirect bandgap Tauc plots of UV-Visible absorption spectra of three BAs crystals. Inset: optical transmission images. (b) Room temperature PL spectra of the samples. (c–d) Evolution of PL of a BAs as a function of temperature (c) from 17 to 212 K and (d) from 212 to 300 K.

edge. The intersections give us a bandgap of 1.82 eV, which falls in the range of the latest DFT calculations [11–14].

Compared to UV-Vis, PL is more sensitive to the crystal quality, defects, and doping levels [23]. Because the recent high κ demonstrations are actually successful stories of material synthesis of high-quality BAs crystals, we performed PL spectroscopy at room temperature although earlier BAs samples exhibited no PL at all [27]. Despite being an indirect semiconductor, the samples reported here show very strong PL as displayed in Fig. 1b, indicating a much better crystal quality. The spectra feature a high energy peak at 1.72 eV and a relatively weak peak at 1.4 eV. A close comparison between the PL and absorption spectra reveals a close relationship: Sample #1 with a weak absorption below the absorption edge exhibits a dominant PL peak at 1.72 eV, while Samples #2 and #3 with stronger absorption at the absorption tails also exhibit a strong PL at the same energy. We conclude that the 1.72 eV peak is the band-edge–associated PL. The 1.40 eV peak comes from sub-bandgap defect states, which is believed to be responsible for the observed bandgap values in earlier reports [3,17,18].

The room temperature PL in Fig. 1b has less spectral features than that of recently observed PL at 10 K which was claimed to be dominated by defect-bound excitons, donor-acceptor transitions, and free exciton transition observed only under a strong excitation [12]. To complete the PL spectra comparison, we varied the temperature and monitored the evolution of PL. As can be seen from Fig. 1c and d, the PL at 17 K resembles the reported features very well in a study by Lyons et al. [12] and confirms the peak at 1.72 eV as owing to band-edge free exciton transitions. As temperature increases, the intensity of all three major peaks decreases and begins to merge. At ~160 K, the bound exciton peak is merged into the free exciton peak. At ~260 K, the donor-acceptor transition peak disappears. The disappearance of these peaks at higher temperatures is due to thermal excitation of loosely bound electrons and holes. In contrast, the intensity of the defect state at 1.40 eV changes very little, proving that it is from a different origin.

Based on well-established relationship between PL and crystal quality and the relationship between crystal quality and thermal conductivity κ proved by recent demonstrations and theories [4–8,23,28,29], we speculate that a strong PL must lead to a high κ. To make use of these relationships for thermal conductivity measurement, we take one step further and utilize confocal PL imaging to evaluate κ of large BAs crystals. Fig. 2 shows the optical pictures and PL-mappings of three BAs crystals at room temperature. The PL-mapping was performed with a custom confocal laser-scanning fluorescent microscope using a 532-nm 40-mW pulsed diode laser to raster scan the sample surface and a GaAsP photomultiplier tube (PMT) with sensitivity in the range of 300–720 nm. A 635-nm long-pass filter was used to block PL excitation. Depending on the mapping size and resolution, PL-mappings of millimeter-sized samples takes seconds or less to complete, and a real-time PL-mapping is also easy to achieve. Despite apparent single-crystal sample, PL-mappings reveal a non-uniform intensity (Fig. 2b and d) across the smooth surfaces (Fig. 2a and c), which indicates a non-uniformity of crystal quality in the same crystalline surface. PL-mapping further reveals very different domain patterns (Fig. 2f and h) on the opposite surfaces of the same BAs crystal (Fig. 2e and g). The measured κ values shown in Fig. 2d will be explained in details in the next paragraph.

To obtain a quantitative κ and experimentally verify the relationship between κ and PL, we further developed an optical technique that is convenient and compatible with PL and requires no extra sample preparation. Fig. 3a shows the schematic of TDTP. In parallel to TDTR [19–21], TDTP uses a pump pulse (527 nm, 140 ns) to generate localized heat in a sample, and a weak time-delayed probe pulse (527 nm, 100 ns) to monitor the temperature and heat transfer dynamics. κ is obtained by fitting the measured temperature data to the known analytical/numerical solutions. However, there are very distinct differences between TDTP and TDTR. Instead of ultrafast femtosecond or picosecond lasers used in TDTR, TDTP uses nanosecond lasers which are much cheaper and accessible. The local heat in the material is directly generated by the material's optical absorption of pump pulse, so there is no metal film coated on the surface as in TDTR. The temperature of the sample is obtained by its temperature-dependent PL. To eliminate the PL excited by the pump, the probe pulses are modulated, and the PL is detected at the probe modulation frequency.

Temperature affects the PL spectrum of a material in many ways; conversely, the spectral changes can be used to measure a sample's temperature [30]. Fig. 3b shows an example of temperature PL shift. The spot P1 was chosen from sample No. 5 as shown in Fig. 2c and d. The spectrum from spot P1 is shown in Fig. 3b. As the temperature increases, the PL peak intensity remains the same, but the short wavelength spectral region becomes enhanced (Fig. 3b). We believe this is due to increased rate of optical transitions of thermally excited electrons and holes that involve absorption of phonons around the indirect bandgap [23,31]. To use this

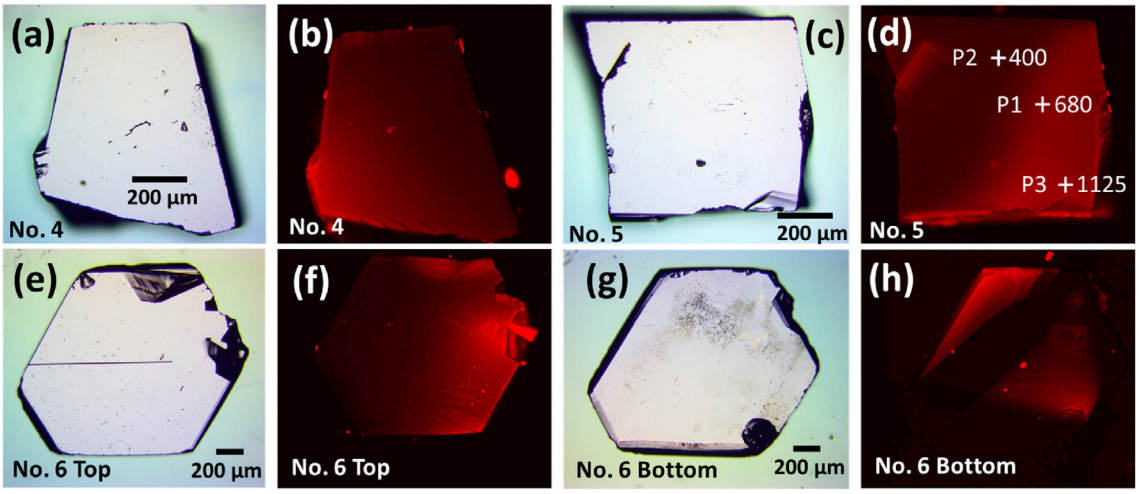

Fig. 2. PL-mapping of three BAs samples. Optical images (a, c) and PL-mappings (b, d) of samples No. 4 and No. 5. The selected spots P1-3 are marked by "+" along with their κ measured with TDTP. Optical images (e, g) and PL-mappings (f, h) of opposite surfaces of sample No. 6.

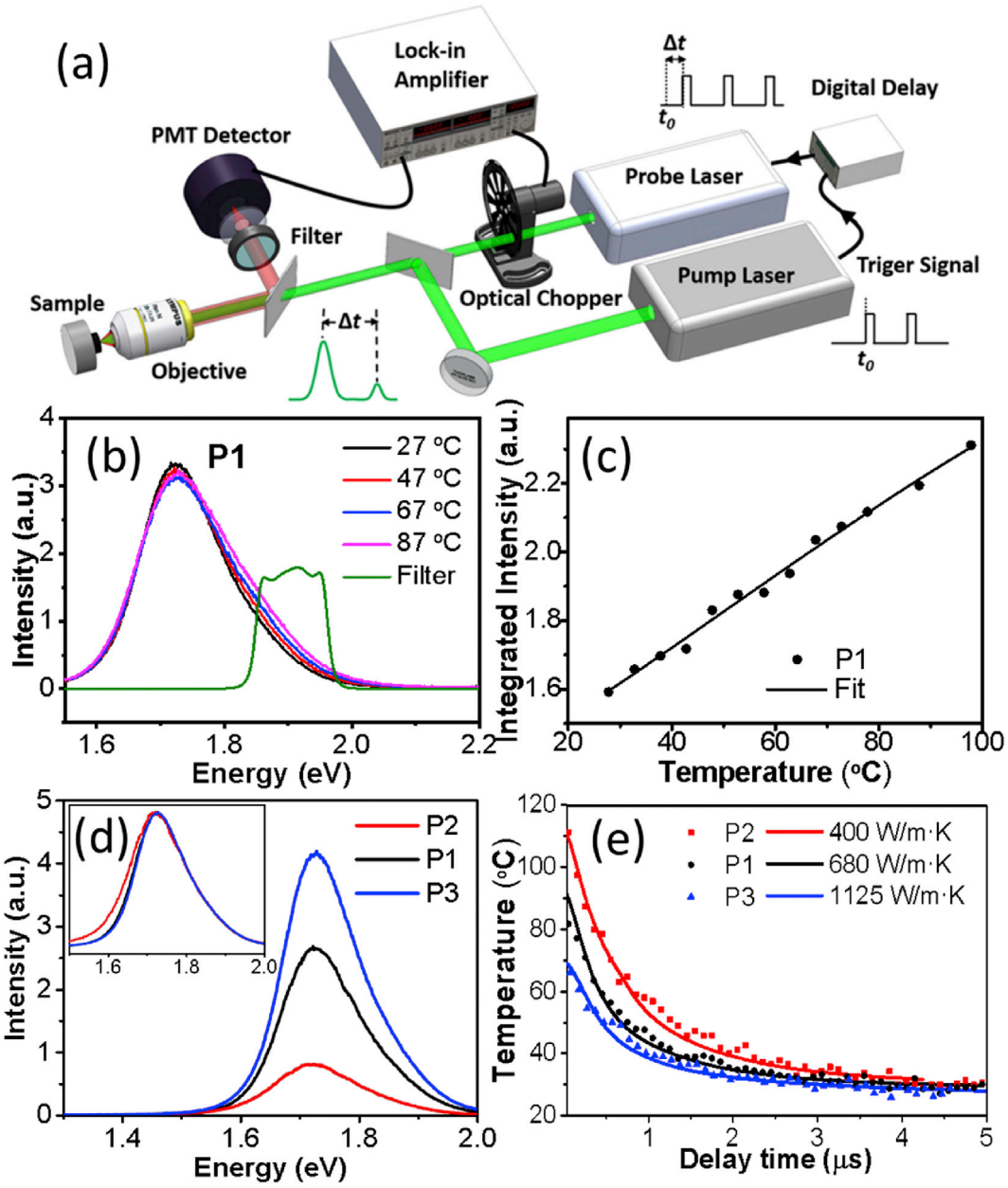

Fig. 3. Time-domain thermo-photoluminescence (TDTP). (a) Schematic of TDTP. (b) Temperature-dependent photoluminescence spectrum of the spot P1 in Fig. 2c and d, and the transmission spectrum of a filter used to select the spectral window for TDTP. (c) PL intensity integrated over the transmission window as a function of temperature. (d) Photoluminescence spectra of spots P1, P2 and P3 as shown in Fig. 2c and d. (e) TDTP traces for P1, P2 and P3, and simulated curves.

temperature-dependent PL spectrum as a sensitive temperature marker in TDTP, we use a band-pass optical filter to select a short wavelength band and then use a fast PMT to measure the integrated intensity over that band. The spectrum of that band is shown in Fig. 3b and c shows an almost linear dependence of the integrated PL intensity as a function of temperature; this same curve will be used to determine the sample temperature.

To make a good comparison and estimate for the whole sample, we chose two more spots P2 and P3 from the PL-mapping in Fig. 2c and d. Fig. 3d shows their PL spectra; note that the spot with stronger PL also has a narrower PL line width. Fig. 3e shows their TDTP temperature evolutions. It is very clear that the spots P1 and P3 have lower average temperatures, indicating higher κ values. The temperature differences among the three spots are the greatest right after the excitation of pump pulse owing to their different κ values, and both the temperatures and their differences drop quickly in a few μs owing to fast heat diffusion. Using any commercial heat transport software, we can fit TDTP curves with κ as a parameter. The simulation results with SIMULIA ABAQUS or COMSOL (See supporting file for details) shown in Fig. 3e give us a room-temperature κ of 680 W/m·K for the stronger PL spot P1 and 400 W/m·K for the weaker PL spot P2 (their spot locations are shown in Fig. 2d). The highest κ corresponding to the strongest PL spot P3 in Fig. 2d reaches 1125 W/m·K, in agreement with the recent demonstrations by TDTR [6–8]. It should be noted that although recent four-phonon scattering theory has reduced the predicted thermal conductivity from 2200 to 1400 W/m·K, its calculations are very computationally expensive and are difficult to be verified through experiment or other methods [32]. In addition, the theory has never accounted realistically for phonon-defect

scattering in BAs and that its most accurately predicted κ-values are for crystals that still show the signature of defects.

Having shown the power of PL-mapping and TDTP, we note that some region of the sample No. 6 in Fig. 2g and h exhibited weak or no PL even though it was grown by the same recently reported method [24]. In fact, our early BAs samples before this work also exhibited no PL [27]. Because TDTP is not applicable to samples without PL, we developed another technique that requires little sample preparation as PL-mapping and TDTP to quickly prove that samples with no PL have a much lower κ. Fig. 4a shows the experimental setup. Here a continuous wave (CW) laser is used to induce local heating, and an infrared thermal camera is used to monitor the temperature evolution directly. To have a good comparison, we chose three samples with similar sizes and thickness. Fig. 4b shows their optical images, and their PL spectra are shown in Fig. 4c; Sample No. 7 was from our early batch that does no show PL [27]. The other two were recently grown [24], but sample No. 9 has a much stronger PL than No. 8. Fig. 4d shows that, for all three samples, the temperature at the laser focus point increases quickly initially and eventually reaches a plateau. Simulation with COMSOL (See supporting file for details) gives us thermal conductivity κ of 160 W/m·K for sample No. 7. Fig. 4e shows snapshots of surface temperatures for the three samples at 40 ms; a much high temperature and large temperature gradient at the laser spot on the sample No. 7 is seen, further confirming that the sample with no PL has lower κ owing to poor crystal quality. However, the technique fails to distinguish samples No. 8 and No. 9, both of them reached similar temperatures despite their huge difference in PL intensity. Apparently, this failure is due to the slow mechanical switching of the CW laser, slow millisecond response of the thermal camera, and the simplified boundary conditions that make realistic simulation difficult. Nevertheless, the infrared thermal images in Fig. 4e have allowed us to identify a sample with low thermal conductivity and given us a vivid picture of heat transfer.

The failure of the slow thermal camera for high κ materials reminds us of the importance of detection speed; however, it does not mean necessarily that the faster detection speed results in better data. For most heat transport study as demonstrated by TDTP, nanosecond resolution is sufficient and even perfect from the basic physical consideration because this is the time for photo-excited carriers to fully relax and reach thermal equilibrium with lattice, so that the actual temperature of lattices can be accurately probed by nanosecond PL. This is also true from practical point of view because for samples with thickness on the order of micrometers, the thermal relaxation time is on the order of nanosecond. Ultrafast lasers are required in TDTR mainly because of ultrafast thermal relaxation of the thin metal film thermal transducer [19–22]. This thermal relaxation time certainly cannot limit the

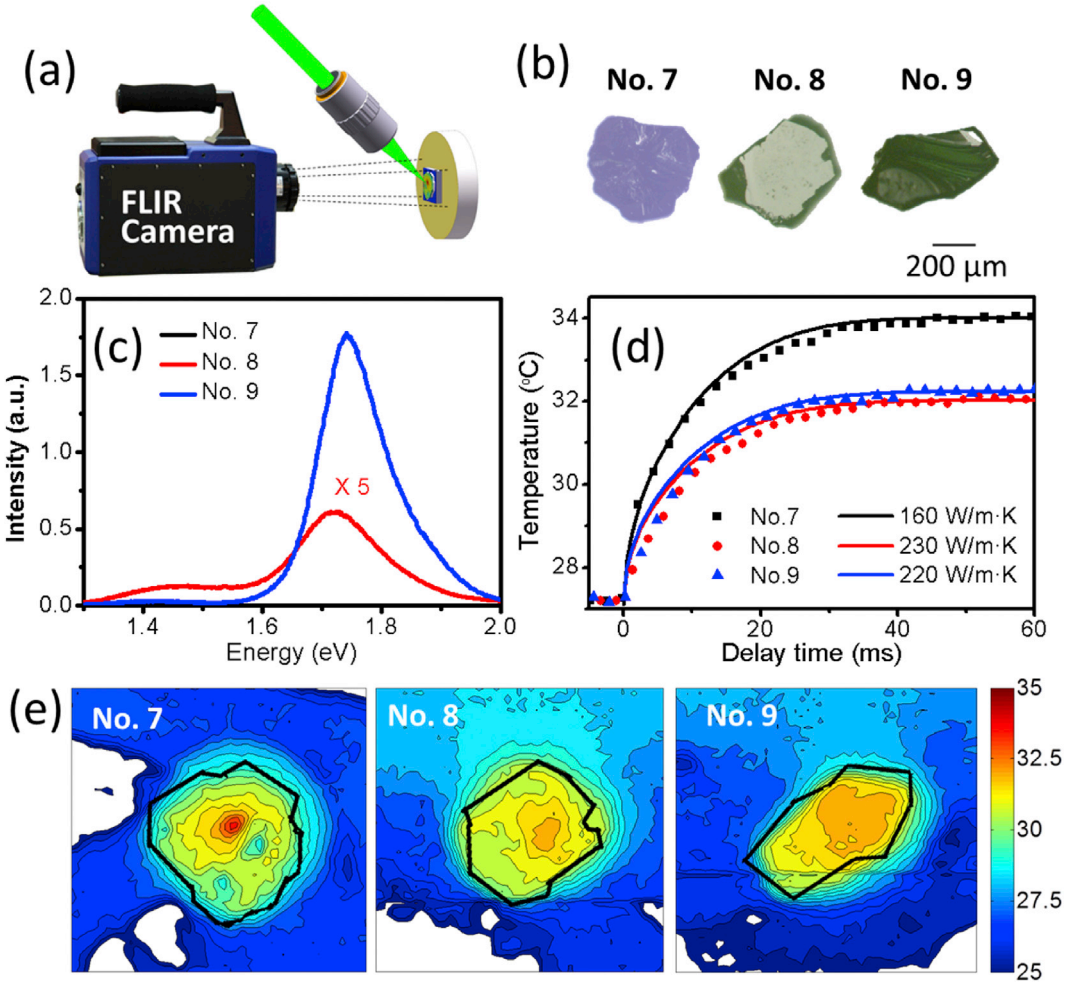

Fig. 4. Comparison of κ using laser-induced heating and infrared thermal imaging. (a) Schematic of experimental setup. (b) Optical images of three samples. (c) Their PL spectra. The PL of No. 7 was not detected. (d) Temperature evolutions of laser spots (hottest spots in Fig. 4e) on the three samples. Dotted lines are data; the solid lines are COMSOL simulations. Laser was turned on at time zero. (e) Contour map of surface temperatures of the three samples at 40 ms. The heating power of a 532-nm continuous wave (CW) laser is 70 mW.

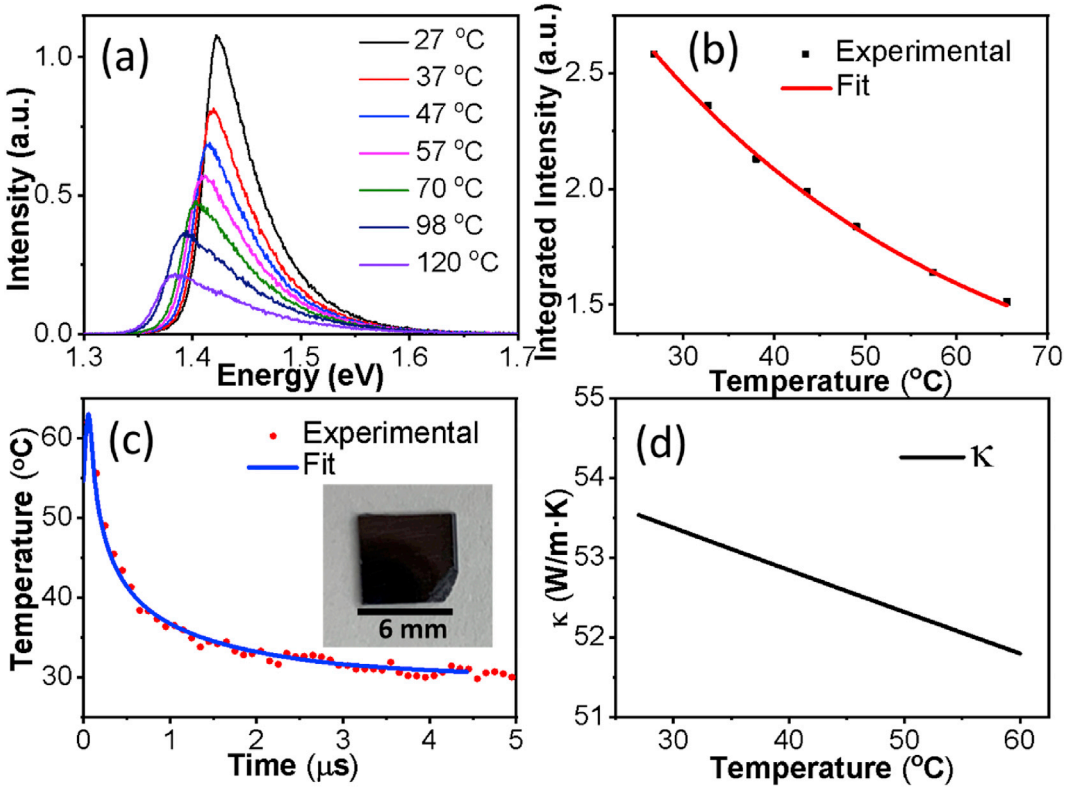

Fig. 5. Thermal conductivity κ of GaAs measured by TDTP. (a) Temperature-dependent photoluminescence spectrum. (b) Integrated PL intensity as a function of temperature. (c) TDTP trace and simulation. (d) Temperature-dependent κ from simulation in (c). TDTP, time-domain thermo-photoluminescence.

application of TDTP. For thin films and even atomically thin 2D materials, we can suspend them or place them on a good thermal-insulating substrate to eliminate out of plane heat loss. Thus, similar to PL and PL-mapping, TDTP can handle most samples, regardless of their size and thickness.

To prove the reliability and accuracy of TDTP, we choose high-quality GaAs as a reference to measure its known κ using TDTP. Because its bandgap is lower than that of BAs, the same 527-nm laser will also work for GaAs. Fig. 5a shows the temperature-dependent PL spectrum of GaAs. At higher temperatures, the PL of GaAs is dominated by the direct band-to-band radiative recombination with energy that follows the temperature dependence of the bandgap. In this case, the total integrated PL intensity is an excellent temperature marker. Fig. 5b shows the integrated PL intensity as a function of temperature measured by the same PMT as for BAs. Based on the TDTP data and simulation in Fig. 5c, we obtained a temperature-dependent κ of GaAs, as shown in Fig. 5d; it agrees well with published values of GaAs [33], which firmly proves that our TDTP method is reliable for measuring the κ of BAs.

Having successfully demonstrated TDTP, we want to stress that TDTP still needs a lot of improvement. Similar to many other optical techniques such as TDTR, there is a lot of room for improvement and refinement that has been going on for many years [22]. For example, the laser pulse width can be reduced to achieve a higher time resolution because of shorter PL lifetimes of BAs and GaAs (Fig. S6). For some materials, the time resolution can be limited by a longer PL lifetime. In any case, it is important to know the response time of PL to achieve an accurate κ especially for materials with high κ. The laser pulse shape and power can be adjusted to make heat generation more accurate and controllable. Similar to PL-mapping, TDTP can be optimized and automated to speed up data acquisition and reduce signal fluctuations. In this demonstration of concept, the experiment was not optimized, and each data were obtained point by point manually; as a result, both temperature calibration and TDTP curves are not smooth, and the simulation fits are also not perfect. However, similar to TDTR, a straightforward analysis of uncertainty is difficult [22]. Experimentally, owing to weaker PL of BAs than GaAs, BAs has a lower quality of TDTP data. Based on preliminary comparisons of simulations and experiments in the supporting materials, as well as the comparison of κ accuracy using GaAs, we believe our measured κ of BAs has a 10–15% uncertainty. The essence of combining PL-mapping and TDTP is that it can quickly screen the crystal quality uniformity and find the highest κ value so that researchers can further refine the growth method to achieve crystals with uniformly high κ for any possible applications.

3. Conclusions

In summary, we have experimentally determined the bandgap of BAs and observed its band-edge PL at room temperature as a measure of crystal quality. We subsequently developed and demonstrated PL-mapping and TDTP as quick and reliable screening methods to measure κ values of semiconductors using nanosecond lasers with little sample preparation. Our PL-mapping technique revealed non-uniformity of κ and different κ domains in apparent single crystals BAs, which allowed us to identify region with highest κ and guide us to improve the growth techniques. TDTP accurately measures the κ of selected spots from the PL-mapping images. As rapid non-contact optical techniques with little sample preparation, PL-mapping and TDTP will greatly accelerate the search for high κ semiconductors for device applications.

Acknowledgements

The work carried out in Z.F.R.'s lab was supported by the U.S. Office of Naval Research under MURI Grant N00014-16-1-2436. J.M.B. acknowledges support from Welch Foundation (E-1728) and National Science Foundation (EEC-1530753). S.Y acknowledges support from China Postdoctoral Science Foundation 2019M653367. J.H. acknowledges support from the National Science Foundation (Grant No. ECCS-1809622).

Conflict of interest

The authors declare that they have no known competing financial interests or personal relationships that could have appeared to influence the work reported in this article.

Author statements

S.Y. measured the absorption, PL spectra, temperature mapping and developed the TDTP system with the help of V.T. and S.-Y.D., D.M. measured the PL-mapping. G.A.G., F.T., and H.S. prepared the samples. M.M., Y.D., J.H., and D.L. conducted the simulations.

J.B., Z.R., Z.W., D.L., S.Y., and F.T. designed the research. J.B., S.Y., and F.T. wrote the manuscript; J.B., Z.R., Z.W. edited the manuscript. All authors discussed the data and commented on the manuscript.

Appendix A. Supplementary data

Supplementary data to this article can be found online at https://doi.org/10.1016/j.mtphys.2020.100194.

References

[1] J.A. Perri, S. La Placa, B. Post, New group III-group V compounds: BP and BAs, Acta Crystallogr. 11 (1958) 310.
[2] T.L. Chu, A.E. Hyslop, Crystal growth and properties of boron monoarsenide, J. Appl. Phys. 43 (1972) 276–279.
[3] T.L. Chu, A.E. Hyslop, Preparation and properties of boron arsenide films, J. Electrochem. Soc. 121 (1974) 412–415.
[4] D.A. Broido, L. Lindsay, T.L. Reinecke, Ab initio study of the unusual thermal transport properties of boron arsenide and related materials, Phys. Rev. B 88 (2013) 214303.
[5] L. Lindsay, D.A. Broido, T.L. Reinecke, First-principles determination of ultrahigh thermal conductivity of boron arsenide: a competitor for diamond? Phys. Rev. Lett. 111 (2013): 025901.
[6] F. Tian, B. Song, X. Chen, N.K. Ravichandran, et al., Unusual high thermal conductivity in boron arsenide bulk crystals, Science 361 (2018) 582.
[7] S. Li, Q. Zheng, Y. Lv, X. Liu, et al., High thermal conductivity in cubic boron arsenide crystals, Science 361 (2018) 579.
[8] J.S. Kang, M. Li, H. Wu, H. Nguyen, et al., Experimental observation of high thermal conductivity in boron arsenide, Science 361 (2018) 575.
[9] C. Dames, Ultrahigh thermal conductivity confirmed in boron arsenide, Science 361 (2018) 549.
[10] T.-H. Liu, B. Song, L. Meroueh, Z. Ding, et al., Simultaneously high electron and hole mobilities in cubic boron-V compounds: BP, BAs, and BSb, Phys. Rev. B 98 (2018): 081203.
[11] K. Bushick, K. Mengle, N. Sanders, E. Kioupakis, Band structure and carrier effective masses of boron arsenide: effects of quasiparticle and spin-orbit coupling corrections, Appl. Phys. Lett. 114 (2019): 022101.
[12] J.L. Lyons, J.B. Varley, E.R. Glaser, J.A. Freitas, et al., Impurity-derived p-type conductivity in cubic boron arsenide, Appl. Phys. Lett. 113 (2018): 251902.
[13] S. Chae, K. Mengle, J.T. Heron, E. Kioupakis, Point defects and dopants of boron arsenide from first-principles calculations: donor compensation and doping asymmetry, Appl. Phys. Lett. 113 (2018) 212101.
[14] J. Buckeridge, D.O. Scanlon, Electronic band structure and optical properties of boron arsenide, Phys. Rev. Mater. 3 (2019): 051601.
[15] M. Ferhat, A. Zaoui, M. Certier, H. Aourag, Electronic structure of BN, BP and BAs, Phys. B Condens. Matter 252 (1998) 229–236.
[16] G.L.W. Hart, A. Zunger, Electronic structure of BAs and boride III-V alloys, Phys. Rev. B 62 (2000) 13522–13537.
[17] S.M. Ku, Preparation and properties of boron arsenides and boron arsenide-gallium arsenide mixed crystals, J. Electrochem. Soc. 113 (1966) 813–816.
[18] S. Wang, S.F. Swingle, H. Ye, F.-R.F. Fan, et al., Synthesis and characterization of a p-type boron arsenide photoelectrode, J. Am. Chem. Soc. 134 (2012) 11056–11059.
[19] D. Zhao, X. Qian, X. Gu, S.A. Jajja, et al., Measurement techniques for thermal conductivity and interfacial thermal conductance of bulk and thin film materials, J. Electron. Packag. 138 (2016): 040802.
[20] P. Jiang, X. Qian, R. Yang, Tutorial: time-domain thermoreflectance (TDTR) for thermal property characterization of bulk and thin film materials, J. Appl. Phys. 124 (2018): 161103.
[21] D.G. Cahill, H.E. Fischer, T. Klitsner, E.T. Swartz, et al., Thermal conductivity of thin films: measurements and understanding, J. Vac. Sci. Technol. 7 (1989) 1259–1266.
[22] J. Yang, E. Ziade, A.J. Schmidt, Uncertainty analysis of thermoreflectance measurements, Rev. Sci. Instrum. 87 (2016): 014901.
[23] P.Y. Yu, M. Cardona, Fundamentals of semiconductors, in: Physics and Materials Properties, fourth ed., Springer, 2010.
[24] F. Tian, Z. Ren, High thermal conductivity in boron arsenide: from prediction to reality, Angew. Chem. Int. Ed. 58 (2019) 5824–5831.
[25] G.A. Gamage, K. Chen, G. Chen, F. Tian, et al., Effect of nucleation sites on the growth and quality of single-crystal boron arsenide, Materials Today Physics 11 (2019): 100160.
[26] H. Sun, K. Chen, G.A. Gamage, H. Ziyaee, et al., Boron isotope effect on the thermal conductivity of boron arsenide single crystals, Materials Today Physics 11 (2019): 100169.
[27] B. Lv, Y.C. Lan, X.Q. Wang, Q. Zhang, et al., Experimental study of the proposed super-thermal-conductor: BAs, Appl. Phys. Lett. 106 (2015): 074105.
[28] G. Davies, Radiative processes in bulk crystalline silicon, J. Lumin. 80 (1998) 1–7.
[29] M.A. Green, J.H. Zhao, A.H. Wang, P.J. Reece, et al., Efficient silicon light-emitting diodes, Nature 412 (2001) 805–808.
[30] M. Dramićanin, Luminescence Thermometry: Methods, Materials, and Applications, Woodhead Publishing, 2018.
[31] P. Wurfel, The chemical potential of radiation, J. Phys. C Solid State Phys. 15 (1982) 3967–3985.
[32] T. Feng, L. Lindsay, X. Ruan, Four-phonon scattering significantly reduces intrinsic thermal conductivity of solids, Phys. Rev. B 96 (2017): 161201.
[33] J.S. Blakemore, Semiconducting and other major properties of gallium-arsenide, J. Appl. Phys. 53 (1982) R123–R181.